UCRL-52082

INCOHERENT SCATTERING OF GAMMA RAYS BY K-SHELL ELECTRONS

Guy C. Spitale
Stewart D. Bloom

May 12, 1976

Prepared for U.S. Energy Research & Development Administration under contract No. W-7405-Eng-48

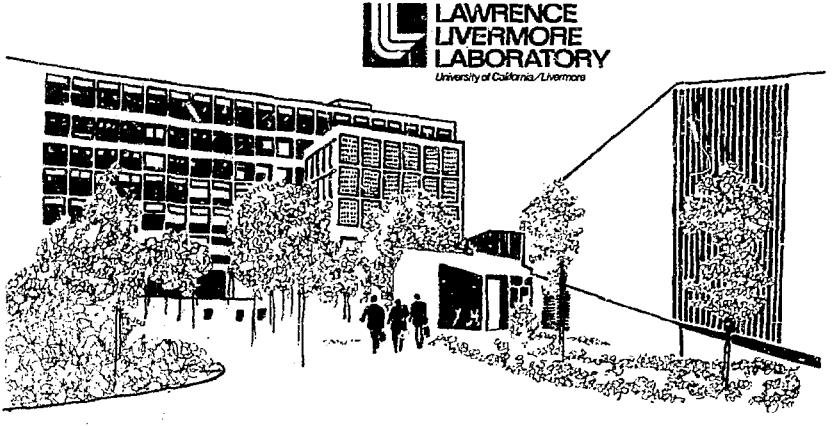

Printed in the United States of America
Available from
National Technical Information Service
U.S. Department of Commerce
5285 Port Royal Road
Springfield, VA 22161
Price: Printed Copy $; Microfiche $2.25

Page Range	Domestic Price	Page Range	Domestic Price
001–025	$ 3.50	326–350	10.00
026–050	4.00	351–375	10.50
051–075	4.50	376–400	10.75
076–100	5.00	401–425	11.00
101–125	5.25	426–450	11.75
126–150	5.50	451–475	12.00
151–175	6.00	476–500	12.50
176–200	7.50	501–525	12.75
201–225	7.75	526–550	13.00
226–250	8.00	551–575	13.50
251–275	9.00	576–600	13.75
276–300	9.25	601–up	*
301–325	9.75		

*Add $2.50 for each additional 100 page increment from 601 to 1,000 pages; add $4.50 for each additional 100 page increment over 1,000 pages.

Distribution Category
UC-34d

LAWRENCE LIVERMORE LABORATORY
University of California Livermore, California 94550

UCRL-52082

INCOHERENT SCATTERING OF GAMMA RAYS BY K-SHELL ELECTRONS

Guy C. Spitale
Air Force Institute of Technology
Dayton, Ohio

Stewart D. Bloom

MS. date: May 12, 1976

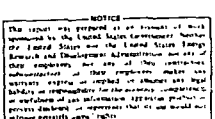

OT W-1405-ENG-48

Contents

INCOHERENT SCATTERING OF GAMMA RAYS BY K-SHELL ELECTRONS

Abstract

Differential cross sections for incoherent scattering by K-shell electrons were measured, using coincidence techniques, for incident photons having energies of 662 keV, 320 keV, and 145 keV. The spectral distributions of the scattered photons emerging at scattering angles from 20° to about 140° are reported. Target materials were iron, tin, holmium, and gold at 320 keV; tin and gold at 662 keV; and iron and tin at 145 keV. A typical energy spectrum consists of a scattered peak that is much narrower than would be expected from the bound state electron motion. The peak also, typically, reaches a broad maximum width for scattering angles between 45° and 60°. Rather than monotonically increasing with atomic number the peak width reaches a broad maximum, generally, between $Z = 50$ and $Z = 67$, and then decreases with increasing atomic number. No Compton defect appears in any of the peaks to within ± 20 keV. A discussion of the expected magnitude of the Compton defect is included. The peak is superimposed on a continuum that diverges at the low end of the scattered photon spectrum for the following cases: gold, holmium, and tin targets for 320-keV incident photons; gold and possibly tin targets for 662-keV photons incident. This infrared divergence is expected on theoretical grounds and has been predicted. It is very nearly isotropic.

I. Introduction

In this work we present experimental results on inelastic (incoherent) scattering from the K-shell of four targets ranging in Z from 26 (iron) to 79 (gold). Three incident photon energies were used — 145 keV, 320 keV, and 662 keV — although not all incident photon energies were used on all targets, due to experimental limitations which are described below. A summary of the targets, sources, and target thicknesses is given in Table 1.

The measurements made in this work were doubly differential, i.e., they are based on energy spectra taken

Table 1. Summary of targets, sources, and target thicknesses.

Source	E_γ, keV	Z	Angle of scatter	Thicknesses, mg/cm^2
^{137}Cs	662	79[a]	20 to 138	26.6, 135, 192
^{137}Cs	662	79[a]	20 to 142.3	17.0, 108, 262
^{137}Cs	662	50	20 to 142	19.6, 62.2
^{51}Cr	320	79[a]	20 to 137.4	26.6, 135, 192
^{51}Cr	320	67	20 to 136	21.9
^{51}Cr	320	50	20 to 136	19.56, 62.2
^{51}Cr	320	26	20 to 137	15.8
^{141}Ce	145	26	20 to 137	15.8

[a]Solid suspension of 75 wt% copper — 25 wt% gold.

between appropriate energy limits (see below) at seven scattering angles ranging from 20° to about 140°. Except at forward angles a quasi-Compton peak could be observed, that is a broadened peak at the free Compton energy. The centroid of the quasi-Compton peak showed no discernible shift from the free-electron value, which for our resolution corresponded to <20-keV shift. The excluded angles were such that the binding energy loss put the Compton peak beyond the spectrum cutoff at forward angles. Angles greater than ≈140° were excluded because of experimental limitations. In addition to the quasi-Compton peak, a continuous spectrum rising at low energies with a roughly 1/k dependence was also observed, most clearly in the case of the 320-keV data. This continuous part of the spectrum can be identified with the expected IRD (infrared divergence) and constitutes an important contribution to incoherent scattering in any case where the photon momentum transfer and the momentum of the K-shell electrons are comparable. It is basically a nonrelativistic effect and has been predicted recently in the nonrelativistic treatment of Gavrila[1] and also in the relativistic calculation of Wittwer.[2] It does not appear in the calculation of Whittingham.[3] In fact, the IRD in incoherent scattering does not appear to have been studied in any published theoretical work prior to Ref. 1 and experimentally it appears the present work is the first instance of its explicit

observation. As will be seen, it can constitute a rather important part of the cross section depending on the scattering angle and the lower-energy limit of the detector. In this work, the presentation of results will emphasize the quasi-Compton peak, when it was kinematically available. Thus, the main, though not the only role of the IRD in this paper is with reference to the attendant error due to the inclusion of its tail, which underlies the quasi-Compton peak. This is discussed in Sec. III.

Although many theoretical calculations have been made of the incoherent Compton process, with the exception of the work of Refs. 1 and 2 no attempt to construct a complete inelastic (off-the-shell) theory has been made, to the knowledge of the present authors. In our case, and indeed for all intermediate photon energies (200-3000 keV), Compton scattering is the dominant effect. In this energy range, a relativistic theory is essential, in which case the results of Ref. 1 are inapplicable. The truncation in angular momentum waves of Ref. 2, which is a relativistic theory, is also an unacceptably severe restriction in our case, as will be shown (see Sec. III). In any case, it is true that a complete calculation would suffer the usual off-the-shell defects (for one example, the loss of gauge-invariance); however, it would have the important advantage of being as realistic as quantum theory now permits. The IRD would be a required (and realistic) result of such a theory, as already noted.[1,2] Furthermore, the effects of a true off-the-shell calculation on the quasi-Compton peak, the main concern of the present experimental work, could be quite significant.

Indeed, the lowering of the forward scattering cross section (as compared to the free-scattering Klein-Nishina result) has been predicted in several incoherent-factor and form-factor theories,[4-6] which is of course one result of the inelastic character of the process. However, other effects might be expected as well, and the experimental observations of our work lead us to the conclusion that at least three other effects do exist that cannot be easily explained without the explicit calculation of off-the-shell matrix elements. One of these is the relative insensitivity of the broadening of the quasi-Compton peak to scattering angle. This effect seems to be coupled with another effect, namely, a dependence of the broadening on Z that shows a rather wide maximum around $Z = 50$. Both of these effects were observed at an incident energy of 320 keV. At 662 keV, on the other hand, the narrowing

of the peak at back-angles (≥100°), as compared with angles ≤60° is very large, in the range 4x to 6x. All these effects are discussed in more detail in the following sections.

There have been a number of experiments reporting the differential cross sections for Compton scattering by the K shell in targets of atomic number varying between 50 and 82.[7-15] The techniques used in most of these experiments[7-12,15] are essentially identical. When a gamma ray is scattered incoherently by an electron in the K shell, the electron is usually ejected from the atom, leaving it in an excited (and ionized) state. The atom decays by emission of a characteristic K x ray with a probability defined by the K-shell fluorescent yield. Photons scattered by the K shell can be distinguished from others by demanding that they be counted in coincidence with accompanying K x rays. This excludes from measurement not only photons scattered by other shells but also coherently scattered photons, since these latter do not leave an exicted atom.

The major variations among preceding experiments are in the quality of the electronics used (of particular significance is the resolution time of the coincidence system), and sources used, the targets exposed, and the geometrical arrangement of source and detector. Nearly all these used the 662-keV line of cesium-137 as a source of incident gamma rays.

The present work was motivated, then, in part, by a desire to investigate the effects of electron binding on the differential cross sections in energy regimes which will likely be treatable with theories in the near future. Chintalapudi and Parthasardhi[12] also reported measurements for 320-keV photons incident on lead, tantalum, and samarium at angles between 30° and 130°. Their results were in radical disagreement with data presented by Pingot[14] for 279-keV photons incident on tantalum and samarium at angles between 70° and 160°. It was our further hope to resolve this conflict, if possible. Since, as already noted, the measured energy-dependent, differential cross sections diverge at low scattered photon energies (the IRD), the energy-integrated cross section will depend strongly on the low-energy cutoff of the apparatus. It is therefore reasonable to attribute the discrepancy between Refs. 12 and 14 to differing low energy thresholds of the respective detection systems. In the present work, the experimental apparatus was generally capable of resolving the quasi-Compton peak due to its sharpness. Another

consequence of this was that we were able generally to characterize the behavior of the width and position of the Compton peak as a function of scattering angle, atomic number, and source energy.

The results of previous experiments of this type have been reported in the form of ratios of measured cross sections for bound electrons to measured cross sections for "free" electrons. The latter cross sections were typically measured for either a beryllium or aluminum target using the gamma-ray leg of the electronic system in a singles mode. The purpose for representing results in this way would be to cancel systematic errors in the absolute value of measured cross sections. In our case, the singles and coincidence experiments were so different (i.e., one detector in singles mode vs two detectors in a coincidence mode) that this type of data presentation served no useful purpose. Accordingly, although singles experiments were performed using aluminum targets as a check, results are reported here in the form of absolute cross sections.

II. Experimental Procedure

A. TARGETS AND SOURCES

The matrix of targets and sources is listed in Table 1. Four elementary targets were used: iron ($Z = 26$), tin ($Z = 50$), holmium ($Z = 67$), and gold ($Z = 79$). The gold targets used at 320 and 662 keV actually consisted of a copper-gold alloy (10 at % gold). At 662 keV, only gold and tin were studied; at 145 keV, only tin. These limitations are discussed in Sec. 2D.

B. METHOD

The experimental method used here was qualitatively the same as that previously used to measure inelastically scattered photons in coincidence with characteristic x rays. The target foil was viewed by two detectors; one was sensitive to characteristic K x rays emitted by the target and the other to scattered gamma rays (see Fig. 1). The signals from these detectors were processed electronically by a slow-fast coincidence circuit (Fig. 2) that counted those events "simultaneously" registered in both detectors. A multichannel analyzer (MCA) stored the record of these events. The calibration of the analyzer in terms of the energy of the scattered photon is described later. The differential

scattering cross sections were then determined from the raw spectra by using the effective source strength, target fluorescence yield, detector efficiencies, and the solid angles subtended by both detectors. The data were corrected for several sources of error (see below).

The apparatus is portrayed in Fig. 1. The incident photon source and associated shielding rested on a stationary platform. Targets were mounted several centimeters in front of the source in such a way that the polar and azimuthal tilt angles could be adjusted. The gamma-ray detector rested on a surface that could be swiveled about the central axis of the target. The x-ray detector was stationed directly above and looking down on the target

The electronic counting apparatus consisted of the usual fast--slow coincidence system. A block diagram is shown in Fig. 2. It was nominally capable of a coincidence window of 10 ns, but was operated at values of between 15 and 20 ns for the purpose of this work. Counts were stored in a 1024-channel analyzer. As usual, the output from the preamp of each detector was split and processed through two separate systems – one a slow system and the other a fast system. In each leg the signal was shaped and amplified by a linear

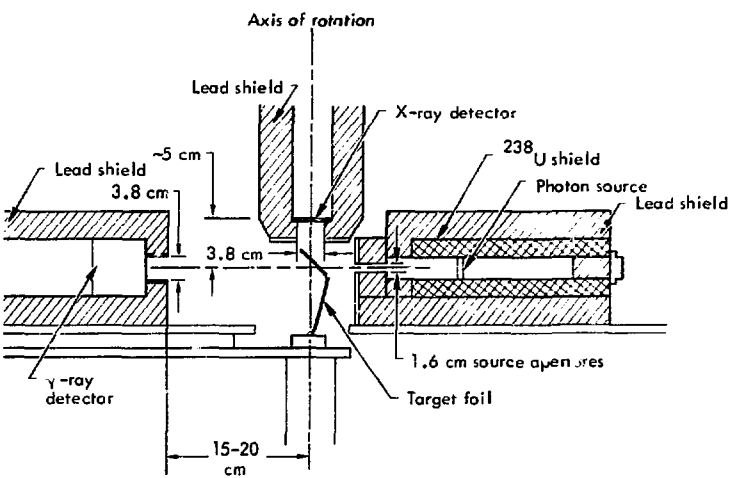

Fig. 1. Experimental apparatus. See Sec. II for a discussion.

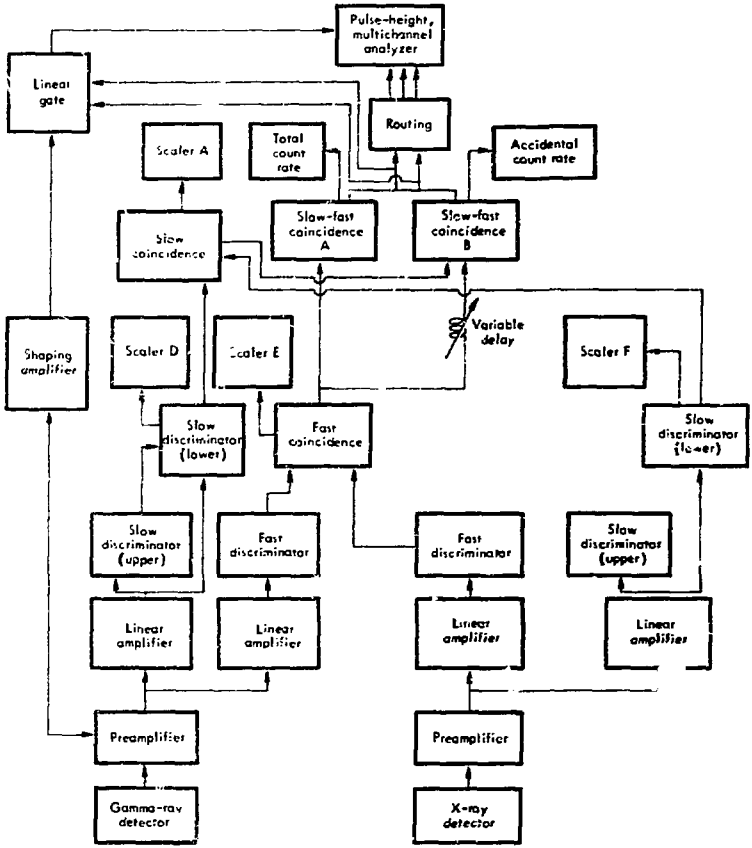

Fig. 2. Electronic slow-fast coincidence system. See Sec. II for a discussion.

amplifier and then subjected to discrimination – either slow or fast as appropriate. The lower limits of the gamma discriminator are shown in Table 2. The output from the slow leg for each detector was fed to a slow coincidence unit ($2\tau \sim 0.5$ μs). Similarly, the output from the fast leg for each detector was fed into a fast coincidence unit ($2\tau \lesssim 20$ ns).

The output from the fast coincidence unit was divided and one signal delayed by approximately 400 ns with respect to the other. Each of these channels was fed to a slow-fast coincidence unit. The output from the slow coincidence unit was also fed into both slow-fast units, which allowed for the simultaneous determination of the real and accidental count rates. Slow-fast coincidence unit A was triggered by both real and accidental coincidences; coincidences registered in unit B were all accidental. The output from each slow-fast unit was in the form of a logic pulse of duration ~0.5 μs that was used as both a gating pulse to sense gamma-ray detector signals enroute to the MCA and as a routing pulse to segregate unit A counts from unit B counts. A determination of the optimal delay between x- and gamma-ray legs was made before and after each change of target or source. The coincidence window, which was determined by the fast system, was set so that the electronic loss of counts was negligible.

C. DETECTOR EFFICIENCIES

Sodium iodide scintillation detectors were selected for both legs of the coincidence system because of their high efficiency and relatively simple operating characteristics. The gamma-ray detector's crystal was 7.62 cm long by 7.62 cm in diam. The photomultiplier was operated at bias voltages between 1000 and 2500 V. The x-ray detector's crystal was 0.32 cm thick by 5.08 cm in diam and was operated at similar bias voltages.

Table 2. Gamma-ray lower discriminator setting in each experiment. $E_S \equiv$ source energy. $E_B(Z) \equiv$ K-shell binding energy. The upper discriminator was always set well above the energy limit, $E_S - E_B(Z)$; see column 4.

Source energy (E_S), keV	Z	Lower discriminator setting, keV	Upper energy limit [$E_S - E_B(Z)$], keV
662	79	160	582
662	50	60	633
320	79	30	240
320	67	80	265
320	50	50	29
320	26	45	313
145	26	20	138

Both detectors were collimated down to a diameter of 3.8 cm for the purpose of minimizing escape effects.

The overall efficiency of the gamma-ray detector was determined by use of calibrated sources and found to be 100% over the energy regimes of interest in the sense that all incident photons were registered by the detector. The photopeak efficiency is discussed in Sec. II.E.

D. BACKGROUND SUPPRESSION

To minimize the rate of accidental counts, several precautions were taken. Both detectors were surrounded by 1-in. thicknesses of lead except, of course, for the required apertures. The radioactive sources were imbedded in a 10-cm cube of depleted uranium-238. This cube was, in turn, surrounded by a 5-cm thickness of lead. The aperture for the escape of source radiation extended 0.32 cm horizontally and 1 cm vertically. Additional movable lead shielding was used to prevent the gamma-ray detector from directly viewing the source slit in various arrangements, depending on angle of scatter. The x-ray detector was always located so that it was not exposed to scattered radiation from the source slit. All lead surfaces in the field of view of the gamma-ray detector were covered by a graded-Z absorber designed to suppress characteristic lead x rays.

Further precautions were necessary to account for the spurious or so-called "false" coincidence count rate. The possible causes of these coincidences, which are quite real, are fairly numerous. An important source of "false counts" derives from the production of free electrons as well as the scattered gamma ray and K x ray. The free electron may emit bremsstrahlung photons and/or ionize other atoms, resulting in the emission of additional K x rays. Both of these are second-order effects which, however, cause a spurious peak to appear at the K x-ray energy in some of the spectra (see Figs. 3a and b). Additional photons may also be produced by the double Compton effect, although this is quite negligible because of the small cross section involved. These byproducts may be registered by either detector and real coincidences can occur from all possible permutations among them. A particularly troublesome case is the simultaneous detection of a K x ray by the x-ray detector and a bremsstrahlung photon by the gamma-ray detector. Spurious counts are also induced by the presence of products and byproducts of other types of events: e.g., Compton scattering by other shells, coherent scattering, photo-electric absorption.

All the mechanisms discussed above are caused by events that occur inside the target foil. The products and byproducts of a scattering event may also interact with the surroundings of the target and detectors and, after multiple interactions, be counted by one of the detectors. Also, a spurious count can be generated by a photon that fires either detector and scatters into the other. This last effect was easily eliminated, however, by the simple artifice of ensuring that neither detector was in the direct field of view of the other.

In general, the dependence on target thickness of the components of the spurious count rate produced by simultaneous detection of a direct product and byproducts of a scattering event will not be the same as that of the true count rate. The contribution to the measured count rate can, therefore, be determined by taking measurements on targets of varying thickness and extrapolating the results to zero thickness, and

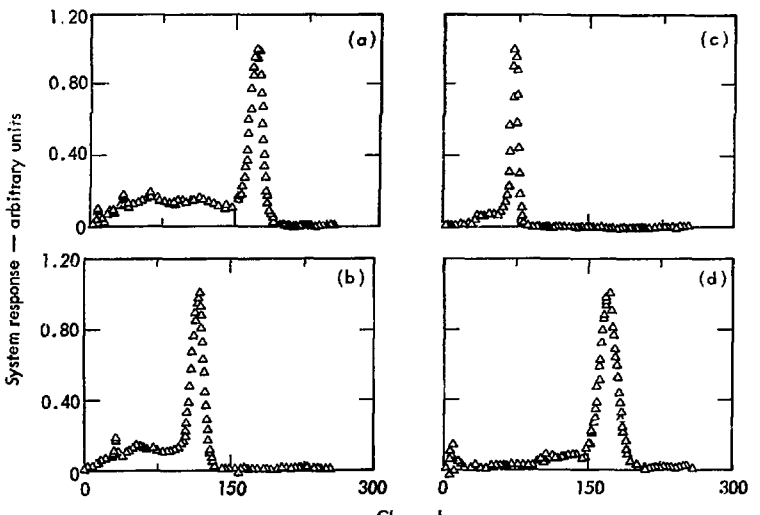

Fig. 3a-d. Typical spectra for 662-, 400-, 225-, and 130-keV incident photons, respectively. Note gains are *not* the same on 3a, b, c, d. The low-energy peaks in Figs. 3a and b are spurious (see Sec. IID).

this was done. Exceptions to this would be contributions due to multiple interactions of photons with the target surroundings and coincidences between Compton electrons and x rays or scattered photons. In both cases, the contribution to the total coincidence rate is independent of target material. The former case arises from the interactions of direct products of Compton events with atoms external to the target foil and is much more dependent on the geometry of the experiment than on the target material. The magnitude of such effects were determined by replacing the target by an equivalent thickness (i.e., a dummy target having the same number of electrons per unit area) of aluminum or beryllium.

In addition to the magnitude of the spurious counts, there is also a contribution to the statistical uncertainty of the final results. In all instances it was found that the spurious rate never exceeded 25% of the total count rate. Thus the contribution to the statistical uncertainty was rather small in all cases. Also, our background was somewhat lower than the average reported in the literature (although East and Lewis[11] report a false rate of about 1 to 2%). This is probably explained by the use of graded-Z absorbers and the fact that the coincidence windows used in this work were several orders of magnitude narrower than those used in all preceding experiments except that of East and Lewis.[11] It was further noticed that placing an 8-mm plastic filter in front of the x-ray detector reduced the false rate to no more than 5% of the total measured rate. The thickness of this filter is greater than the range of 600-keV electrons but still thin enough not to appreciably attenuate the transmission of the photons of interest. A reasonable conclusion, then, would be that most of the spurious count rate was due to coincidences between scattered (and detected) photons and Compton electrons.

E. TRUE COINCIDENCE SPECTRA

The raw experimental data were collected in the form of an array of counts vs channel number in a multichannel analyzer and as shown in Fig. 3. The true count rate (for our purposes) C as a function of channel n is found by correcting for the accidental count rate C_a, the "false" rate C_f, and the false-accidental count rate C_{fa}. It is given by

$$C(n) = C_t(n) - C_a(n) - [C_f(n) - C_{fa}(n)] \quad (1)$$

where $C_t(n)$ is the total count rate

in channel n. The channel number was related to the scattered photon energy E_f by means of energy vs channel calibrations using standard sources. A calibration curve was generated each time the gain of the system was changed. The system was found to be linear to within the limits set by gamma-ray detector resolution.

The relation of the reduced count rate $C(E_f)$ to the doubly differential cross section $d\sigma/d\Omega dE_f$ is given by

$$\frac{d\sigma_c}{d\Omega dE_f} = \frac{C(E_f)/\Delta E_f}{\frac{2S\Omega_b}{4\pi}\frac{\varepsilon_K\Omega_K}{4\pi}\Omega_\gamma\omega_K G_c(E_f)\varepsilon_\gamma(E_f)}, \quad (2)$$

where

$S \equiv$ source strength in disintegrations per second,

$\Omega_b/4\pi \equiv$ relative solid angle subtended by the defining collimator with respect to the source,

$\Omega_K/4\pi \equiv$ relative solid angle subtended by the sensitive area of the x-ray detector with respect to the irradiated area on the target,

$\Omega_\gamma \equiv$ absolute solid angle subtended by the sensitive area of the gamma detector with respect to the irradiated area on the target,

$\varepsilon_\gamma(E_f) \equiv$ efficiency of the gamma-ray detector for energy E_f,

$\omega_K \equiv$ K-shell fluorescence yield,

$G_c \equiv$ geometry dependent factor correcting for absorption within the target (to be discussed later),

$\Delta E_f \equiv$ energy width of a channel.

All these quantities were readily ascertained. The term $[S(\Omega_b/4\pi)\varepsilon_K]$ is actually the "effective" source strength determined by the source calibration procedure, which will be discussed in Sec. 2F. Ω_γ must be small (in this experiment, less than 0.04 sr in all cases) in order to obtain reasonably fine angular resolution. The distance from the gamma detector to the target was always made large compared with the dimensions of the irradiated area. Thus this area could be represented by a point source in calculating Ω_γ. No such constraint influenced the placement of the x-ray detector, and so $4\pi\Omega_K$ was maximized. The point source approximation was inaccurate in this case, but a simple numerical calculation that summed over small differential areas on the irradiated surface for each experiment sufficed to determine $4\pi\Omega_K$. Finally,

ε_γ — the total (as opposed to intrinsic peak) efficiency — was determined as a function of energy by the use of calibrated sources and found to be essentially 100% over all energy regimes of interest (30 to 662 keV). The photoelectric efficiency is discussed next.

The width of the photopeak is influenced both by the solid angle subtended by the gamma detector and by dispersive processes in the detector and supportive electronics. This width, therefore, varied for each experiment but was generally of the order of 10%. Spectral distortion due to photoelectric and Compton escape was minimized by collimation but was still present. Responses of the system to delta function inputs at various energies were recorded and used to deduce the relative photoelectric deflection efficiencies. Radioactive sources and photons scattered by nearly free electrons (i.e., in aluminum) were used as sources for this measurement. Some typical spectral responses are plotted in Fig. 4. As can be readily seen, the Compton edge is relatively unimportant for photon energies less than 300 keV. The dependence of the photoelectric escape peak on incident photon energy was found to adhere to the theoretical optimum described in Siegbahn.[16] The effect of photoelectric escape is negligible at energies greater than 100 keV.

It is clear from the above and Fig. 4 that there is a regime over which the recorded spectra can be used without any spectral correction. This regime happens to coincide with that range of energies over which Compton spectra generated by the 320-keV source are distributed. Accurate determinations of the spectra generated by the scattering of 662-keV photons would require that the measured spectra be mathematically unfolded to compensate for Compton escape processes. This procedure is both difficult and unreliable. The photoescape effect distorts the spectra produced by the 145-keV source, but this can be dealt with by making the reasonable assumption that the width of the escape peak was much less than the separation between the photo and escape peaks. The correction involved is negligible at incident energies above 100 keV but can be sizable below this limit. Because of these uncertainties only the iron data was considered reliable in this case (145 keV).

F. SOURCE CALIBRATION

The effective source strength depended not only on actual strength but also on such things as the solid angle subtended by the aperture in the source collimator, the photopeak efficiency of the x-ray detector, and

the settings of the single channel analyzers and amplifiers in the x-ray leg of the electronics. To account for these factors, the following method of calibration was used. The target was exposed to source radiation collimated as in the actual coincidence experiment. The gain and discriminator value were set and not subsequently altered. The count rate registered in the x-ray detector was then recorded for several positions of the detector. After correction for absorption in the target and in air, the effective source strength S_0 is given by

$$S_0 = \frac{S_k}{\frac{\Omega_k}{4\pi}\,\sigma_p\,\omega_k\,G_k} \qquad (3)$$

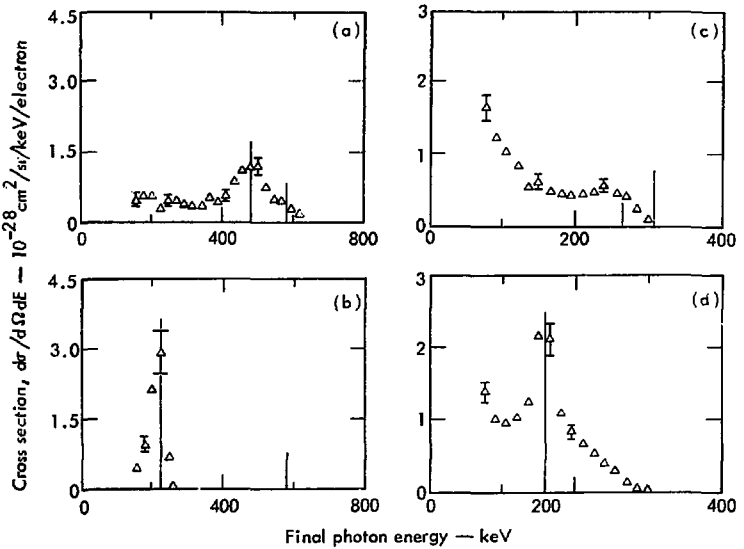

Fig. 4. Doubly differential scattering cross sections vs final photon energies for (a) 662-keV photons incident on gold (Z = 79), scattering angle of 45°; (b) 662-keV photons incident on gold, scattering angle of 120°; (c) 320-keV photons incident on holmium (Z = 67), scattering angle of 20°; (d) 320-keV photons incident on holmium, scattering angle of 136°. The short vertical line represents the high-energy cutoff. The long vertical line represents scattering predicted by the Compton (free-scattering) formula. The solid line in Fig. 4d is the prediction of semiclassical theory (see Sec. III).

where

$S_k \equiv$ count rate of the x-ray detector,

$\Omega_k \equiv$ solid angle subtended by the x-ray detector,

$\sigma_p \equiv$ cross section for photoelectric absorption of source photons,

$\omega_k =$ K-shell fluorescent yield,

$G_k =$ correction for absorption in target.

G. SELF-ABSORPTION CORRECTIONS

In addition to the effects discussed above, the deduced value for $d\sigma/dEd\Omega$ may be influenced by the attenuation of K x rays, scattered gamma rays, and source photons. Necessary self-absorption corrections were incorporated into G_c and G_k as used in Eqs. (2) and (3). Expressions for G_c and G_k for target foils sufficiently thin so that multiple scattering can be ignored can be easily derived. The results are as follows:

$$G_c = \left[\frac{1 - e^{-\sigma_b t_b}}{\sigma_b t_b/\rho t}\right]\left[1 - \left(\frac{1 - e^{-\sigma_s t_s}}{t_s/\rho t}\right)\right]\left[1 - \left(\frac{1 - e^{-\sigma_k t_k}}{t_k/\rho t}\right)\right], \quad (4)$$

$$G_k = \left[\frac{1 - e^{-\sigma_b t_b}}{\sigma_b t_b/\rho t}\right]\left[1 - \left(\frac{1 - e^{\sigma_k t_k}}{\sigma_k t_k/\rho t}\right)\right] \quad (5)$$

where σ_b, σ_s, σ_k are the attenuation coefficients for source photons, scattered photons, and K x rays, respectively; t_b, t_s, and t_k are the effective mass thicknesses of the target foil allowing for its orientation relative to the source beam, gamma-ray detector, and x-ray detector, respectively; and t is the actual mass thickness of the target foil. In the limit of a very thin target foil, G_c and G_k reduce to ρt, and the dependence of these geometric factors on ρt then constitute the necessary corrections for self-absorption. It was found that only negligible corrections G_c and G_k were required in energy regions where the quasi-Compton peaks appeared. However, in the lower energy portions of spectra wherein the IRD dominated the spectrum, significant corrections were required. In the most extreme cases (e.g., scattered photons of energies near 50 keV for 320-keV photons incident on gold or holmium), corrections of the order of 15% were required. Thus G_c and G_k do not contribute significantly to the experimental uncertainty of the final results.

III. Results and Discussion

The results of our measurements are presented in Figs. 4-8 and Tables 3 and 4. In Figs. 4a and b, we give illustrative spectra for forward (45°) and backward (120°) scattering angles in the case of 662-keV photons incident on gold.

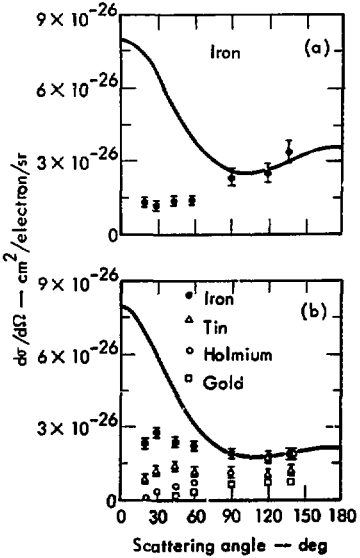

Fig. 5a,b. Area under quasi-Compton peak vs scattering angle for (a) 145 keV photons incident on iron and (b) 320-keV photons incident on various targets. The solid line is a plot of the Klein-Nishina prediction.

Since all the spectra in Fig. 4 have been corrected for background (see above), the continuum in all these figures is largely attributable to the IRD (see below). It clearly contributes to the uncertainty in extracting the area under the quasi-Compton peak, particularly in Figs. 4a, c, and d. In Fig. 4b, on the other hand, the narrowness of the quasi-Compton peak (at 225 keV) makes the contribution of the IRD negligible. In Fig. 4c [320-keV photons

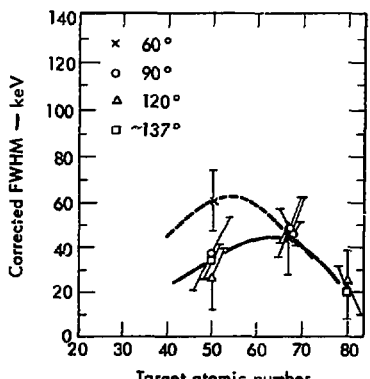

Fig. 6. Corrected FWHM of quasi-Compton peak vs target atomic number for 320-keV incident. The data for $Z = 26$ are not shown because of their very large uncertainty (see Table 4). The curves are intended to guide the eye only.

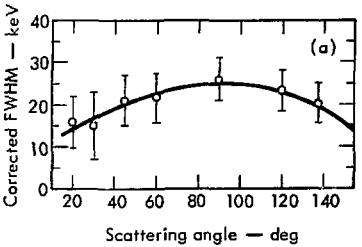

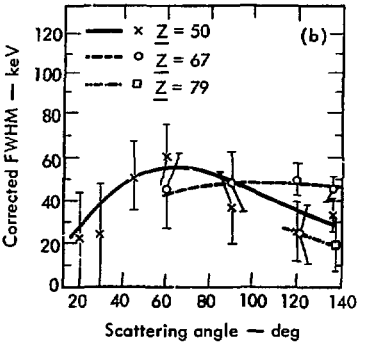

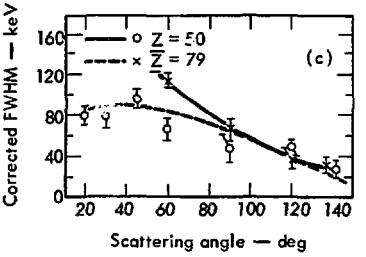

Fig. 7a-c. Corrected FWHM of quasi-Compton peak vs scattering angle for (a) 145 keV incident and $Z = 26$, (b) 320 keV incident and $Z = 79$, 67, and 50, (c) 662 keV incident and $Z = 50$ and 79. The curve is intended to guide the eye only.

incident of holmium ($Z = 67$), $\theta = 20°$], the quasi-Compton peak is eliminated by the binding-energy requirement, and the contribution of the IRD is both dominant and obvious. In Fig. 4d, the same as Fig. 4c except $\theta = 136°$, the quasi-Compton peak is available energetically, quite narrow, and very apparent. However, unlike Fig. 4b, the contribution of the IRD in Fig. 4d is very apparent. This is because the photon momentum transfer and the K-shell electron momenta are in this case the same range: about 0.5-1.5 in natural units ($\hbar = c = m = 1$). Thus the competitive nature of the cross sections for the IRD and the quasi-Compton scattering is to be expected. In all cases, the measured cross section will depend on the lower discriminator setting such that the lower the setting, the higher the cross section. The 320-keV data are more sensitive in this regard than the 662-keV data, as might be expected.

Because, hitherto, the IRD in inelastic Compton scattering has not

been observed (or identified), we took special pains to eliminate all possible spurious sources that might account for the low-energy continuum. Of particular concern was the fact that photoelectrons ejected from the K shell would lead to bremsstrahlung photons that would be in true coincidence with characteristic K x rays. This would be a source of "false"

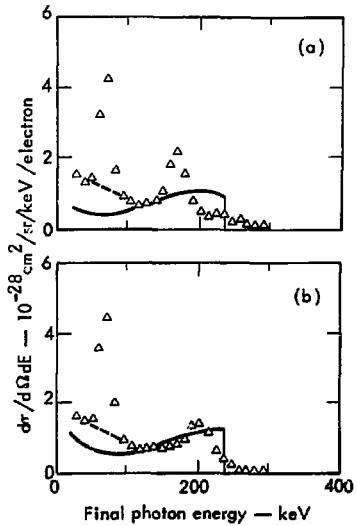

Fig. 8a,b. Prediction of Ref. 2 (Wittwer solid line) compared to experimental data for (a) 320-keV photons incident on gold at 120° and (b) 320 keV photons incident on gold at 90°. Peak at 70 keV is due to spurious coincidences.

coincidences which could not be distinguished from "true" coincidences by, for example, repeating the experiment using an aluminum target. Also, such a contribution would qualitatively resemble our observed IRD in both spectral and angular distribution. Since photoelectrons would initially carry an energy equal to the source energy minus the target's K-shell binding energy, the corresponding bremsstrahlung spectrum will consist of a divergence with a cutoff at the maximum electron energy. This would be identical to that of our observed IRD. Since photoelectrons are emitted isotropically in the center of mass and since the center-of-mass and laboratory frames for high-Z target atoms are practically identical, one would expect the resulting bremsstrahlung to be isotropically distributed. We see some

Table 3. Width of quasi-Compton peak for 145-keV incident. Only the iron data were usable in this case (see Sec. II).

θ_s, deg	Corrected FWHM, keV
20	16 ± 6
30	15 ± 8
45	21 ± 6
60	22 ± 6
90	26 ± 5
120	23 ± 5
137.4	20 ± 5

Table 4. Width of quasi-Compton peak for 320-keV incident.

θ_s (deg)	Corrected FWHM, keV			
	$Z = 79$	$Z = 67$	$Z = 50$	$Z = 26$
20	a	a	22 ± 22	23 ± 22
30	a	49[b]	24 ± 24	25 ± 25
45	a	52[b]	51 ± 16	35 ± 15
60	a	45 ± 18	61 ± 14	38 ± 12
90	26[b]	49 ± 14	37 ± 17	22 ± 14
120	25 ± 14	50 ± 8	26 ± 14	24 ± 9
136		46 ± 6	34 ± 8	
137				17 ± 8
137.4	20 ± 12			

[a]Peak suppressed by kinematics.

[b]Peak eroded by kinematics.

anisotropy in the IRD in our experimental data, but probably not to such a degree that bremsstrahlung could be summarily eliminated as a possible cause of the observed IRD without further considerations.

Shimizu *et al.*[10] estimated the bremsstrahlung effect to constitute a negligible contribution to their observed cross sections. We undertook an independent estimate to verify this. Using the expressions presented in Heitler,[17] we estimated the ranges of Compton electrons of energies concerned in cases exhibiting strong IRD and found these to be of the order of 10^5 mg/cm^2, which is to be compared with foil thicknesses of approximately 20 mg/cm^2. On this basis, we estimated that not more than 0.02% of the emitted K-shell electrons produced bremsstrahlung photons. This is to be contrasted with an observed IRD of magnitude greater than ten times the area under the quasi-Compton peak. Clearly, the bremsstrahlung are quite negligible for our purposes.

We then turned our attention to coincidences between bremsstrahlung photons and K x rays emitted by atoms excited by electrons freed by photoelectric events. Although this is a higher-order effect, the presence of great numbers of photoelectrons makes it a possible cause of bremsstrahlung background. Using a procedure similar to that described above, we estimated that this effect would produce a bremsstrahlung background of

no more than 0.8% of the quasi-Compton peak. Although there may be numerous other processes that result in coincidences between bremsstrahlung and K x rays, they are obviously of higher order than the processes considered above, and thus can be disregarded.

Finally we sought experimental verification of the foregoing analysis. The considerations above indicate that, at least for target foils thin compared to Compton electron ranges, the relative bremsstrahlung background is linearly dependent on target thickness. Thus we examined spectra produced by target foils of widely varying thickness. In particular, we compared spectra produced by gold targets of thickness 200, 100, and 20 mg/cm^2 for source energies of 662 keV and 320 keV at several scattering angles. We also examined spectra produced by target foils composed of an alloy of copper and gold (25 wt% gold) under the same experimental conditions. To within ± 10%, there was no difference in the magnitude of the observed IRD relative to the quasi-Compton peak. This confirmed the conclusion based on calculations (see above).

Although no complete relativistic calculation of the inelastic Compton process is available, a rough estimate can be made of the IRD cross section using the approach of Heitler in the calculation of the production of bremsstrahlung.[17] In this case we combine the photoelectric cross section with the appropriate second-order correction, which then leads to the IRD cross section. In doing this, we assume that the IRD is angularly isotropic. The crude approximation that results is

$$\frac{d\sigma_c}{d\Omega\, dE} \approx \frac{\alpha}{\pi} \cdot \frac{\sigma_{PE}}{4\pi\, E} \qquad (6)$$

where E is the final photon energy, σ_{PE} is the appropriate photoelectric cross section (both energy- and Z-dependent), and α is the fine-structure constant. The factor α/π is part of the second-order correction to the photoelectric effect, which the observed IRD in the inelastic Compton scattering must exactly equal in magnitude and dependence energy (E). This argument is precisely the same that applies to the cancelling second-order corrections in each of the two phenomena, Coulomb scattering and bremsstrahlung.[17]

Applying Eq. (6) to the best case for our purposes, namely the scattering of 320-keV photons from holmium (Z = 67) (see Fig. 4c, d), we find that the ratio of the IRD's observed doubly differential cross section to that predicted by Eq. (6) is in the range 1.0 ± 0.5. (The energy range

and angular range used to obtain this result were 45 keV to 90 keV and 20° to 136°, respectively.) In view of the very rough nature of Eq. (6), the agreement even to within a factor of two must be in part fortuitous. What cannot be fortuitous, however, is the order of magnitude of the predicted IRD. Not only does it agree with our findings, but it could not be negligible.

In Fig. 5, we show the dependence on scattering angle of the cross section for the quasi-Compton scattering at two energies, 145 keV (Fig. 5a) and 320 keV (Fig. 5b). (At 145 keV, only the data for the lightest target — iron — were usable.) In both cases, the measured cross section fell off markedly at forward angles compared with the Klein-Nishina (free-electron) prediction. Such a difference is to be expected from a simple semiclassical model that uses the Klein-Nishina formula in conjunction with the expected momentum distribution of the K-shell electrons.[18] This model was employed by Motz and Missoni,[15] and we have used essentially the same model to make similar calculations to understand, at least qualitatively, the results in Fig. 5 (and also the following figures). In consonance with the finding of Ref. 15, our calculations show that, at forward angles, only the electrons having momentum components that are both large compared to the main segment of the available momentum distribution *and* anti-parallel to the incident photon direction will contribute to the inelastic scattering. This double limitation produces a much reduced cross section. However, since the model, in addition to being elastic, also neglects the Coulomb scattering in the intermediate state (after absorption of the incident photon), it tends to underpredict the forward scattering. Thus, for one example, the cross section cannot be expected to disappear at 0° even using the semiclassical (elastic) model, although it will be much smaller than the free-electron prediction, of course, as was found experimentally. Two other failures of this model are its inability to deal correctly with the Compton shift (see below) and, of course, the total absence of an IRD. Both of these failures can be expected from the completely elastic character of the calculation, and a good example of them is the scattering of 320-keV photons from holmium ($Z = 67$), as shown in Fig. 4d.

The cross-sections for tin and gold at back-angles ($\theta > 90°$) in Fig. 5b are also consistent with the semiclassical prediction in that the cross section is significantly smaller than the Klein-Nishina free-electron prediction, by a factor of

two or so. Furthermore, this discrepancy becomes even more marked with increasing atomic number.[18] However, this statement also has only qualitative validity, as can be seen from the relative behavior in Fig. 5b of the experimental points for holmium ($Z = 67$) and tin ($Z = 50$). The former is essentially at the Klein-Nishina limit, while the latter is down by a factor of 1/2 for $\theta > 120°$. This illustrates the need for a more realistic theoretical formulation of the problem. It is certainly not clear how such detailed behavior can be explained otherwise.

In Figs. 6, 7a, 7b, and 7c are plotted our experimental results for the corrected FWHM of the quasi-Compton peak. The method of correction is described in Sec. II. The same results are given numerically in Tables 3, 4, and 5. The results shown in Figs. 6, 7a, and 7b are consistent with an angularly independent (within a factor of two), but highly Z-dependent FWHM, for 320-keV incident photons. The apparent peaking of the FWHM around $Z = 50$ to $Z = 67$ in Fig. 7, again, cannot be explained without a more complete theory. Also, neither the relative angular behavior nor the absolute values of the FWHM values in Fig. 7c (662-keV incident on targets of $Z = 50$ and $Z = 79$) are predicted correctly by the semiclassical model, which not only require peaks at least twice as broad but also an *increase* of the FWHM with scattering angle, as might be expected from purely classical considerations.

In Figs. 8a and b, we show a comparison between our experimental results and the relativistic calculation of Wittwer[2] for an incident photon energy of 320 keV and a gold target ($Z = 79$). This calculation was truncated to include only dipole and quadrupole emission and absorption. It is not surprising, therefore, that the Compton peak is practically indiscernable in the theoretical curve of Fig. 8a ($\theta \approx 120°$). However, the theory agrees quantitatively quite well with the experimental cross sections when averaged

Table 5. Width of quasi-Compton peak for 662-keV incident.

	Corrected FWHM, keV	
θ_s, deg	$Z = 79$	$Z = 50$
20	a	78 ± 9
30	a	77 ± 12
45	106[b]	95 ± 10
60	115 ± 8	66 ± 13
90	66 ± 11	49 ± 14
120	40 ± 10	50 ± 14
137	34 ± 8	
142		30 ± 9

[a]Peak suppressed by kinematics.

[b]Peak eroded by kinematics.

over about 100-keV intervals, excluding the spurious peak at 70 keV. This same spurious peak obscures the IRD in the experimental data, and so it is not possible to compare theory and experiment in the low-energy region. As already noted, however, the theoretical calculation does continue to rise (towards $E_f = 0$) with a $1/E_f$ dependence in the low-energy region.

We reserve to the last the discussion of the apparent lack of any Compton defect in the centroids of all the quasi-Compton peaks that could be located with any precision. In *no* case did the quasi-Compton peaks shift noticeably from the expected free-electron. Since in all cases our resolution was 20 keV or better, in none of these cases was the Compton defect 20 keV or more. (In a few cases our resolution was ≈10 keV.) Using the well-known low-energy prediction for a shift in wavelength (λ), this shift would be a wavelength change ($\Delta\lambda$) on the order of $|\epsilon_k|/k^2$,[19,20] where $|\epsilon_k|$ and k are the K-shell binding energy and incident photon wave-number respectively, in natural units. In the case of 662-keV photons incident on a gold target ($Z = 79$), this would amount to a lowering of the scattered energy of about 50 keV, much greater than the largest shift in our experiments would have been. In the appendix we present a short resume of formulae and a few calculated results for the centroid shift based on the semiclassical model wherein the low-energy approximations are lifted. For all the cases reported here, the application of the results of the formulae in the appendix lead to the prediction that the largest energy shift will be ≲5 keV and not necessarily in the downward direction. In any case, this limit is at least twice the precision with which we can ascertain the centroid position in our experimental results. It thus appears that the semiclassical model can be successfully applied to the *average* energetics pertaining to the Compton process, regardless of whether it is inelastic. However, beyond this, its usefulness is quite limited, as described above.

IV. Acknowledgments

The authors would like to thank Rex Booth and K. J. Tirsell for technical assistance and advice. We would also like to express our appreciation to Dr. Leon Wittwer for making available the results of his theoretical calculation.

Appendix: The Compton Defect

The Compton defect, a shift towards a longer wavelength for the photons from bound electrons, as compared with free-electrons, has been known for more than forty years. The phenomenon was shown to be a binding-energy effect in 1934 by Bloch[19] in what we call the low-energy limit (see Eq. A6, below). A review of similar treatments as well as measurements (up until 1955) was given by Evans.[20] In this appendix we summarize some calculations on the Compton defect based on the semiclassical model described in Sec. III and in Ref. 15. Our considerations are limited to K-shell inelastic scattering and our purpose is to remove the low-energy approximation so as to discover what happens in more general situations, such as one of concern in the present work, where the photon and electron momenta are not only comparable but relativistic. Using momentum and energy conservation the following formulae can be derived:

$$k' = \frac{f_1 k}{[f_2 + k(1 - \cos\theta)]} \tag{A1}$$

$$f_1 \equiv \frac{(k + \varepsilon_0)(2 + k + \varepsilon_0) - (\langle p \rangle)^2}{2\langle p \rangle} \tag{A2}$$

$$f_2 \equiv \frac{k(1 + k + \varepsilon_0 - \langle p \rangle)}{\langle p \rangle} \tag{A3}$$

where we have used natural units ($\hbar = m = c = 1$) and,

$k \equiv$ initial photon energy (A4a)

$k' \equiv$ final photon energy (A4b)

$\theta \equiv$ photon scattering angle (A4c)

$-\varepsilon_0 \equiv$ initial K-shell electron binding energy $\approx Z^2\alpha^2/2$ (A4d)

$\langle p \rangle \equiv$ the average magnitude of the *initial* total "microscopic" momentum; i.e., the magnitude of the vector sum of the initial photon momentum and the electron momentum averaged over all the directions and magnitudes characterizing the K-shell distribution. (A5)

These results are based principally on the assumption that the replacement of $\langle p \rangle$ with p in Eqs. (A1-3), plus subsequent averaging over all p (see Eq. A5),

will yield the same result. The low-energy limit of Eqs. (A1,2,3) is easily defined and calculated:

Low-energy limit: $|\varepsilon_0| << k << 1$ (A6)

$$\Delta\lambda \equiv \lambda' - \lambda \approx (1 - \cos\theta)\left(1 - \frac{|\varepsilon_0|}{2k^2}\right) + \frac{5}{4}\frac{|\varepsilon_0|}{k^2}$$

where λ and λ' are the initial and final photon wavelengths, respectively, in natural units. If we assume the correction factor $(1 - |\varepsilon_0|/2k^2)$ multiplying the angular term $(1 - \cos\theta)$ is unity, the result is essentially the same as the correction $(\lambda)^2|\varepsilon_0|$ derived by Bloch and others.[19,20] The neglect of the correction to $(1 - \cos\theta)$, however, is justifiable only when $(\lambda)^2|\varepsilon_0|$ is $>>1$ and/or $\cos\theta \approx 1$ (forward angles). These conditions, even in the low-energy limit, are frequently not satisfied.[20]

The next case we treat is more general in that it is based on the assumption that only the energy of the photon is restricted, so that its momentum will be large compared to that of the initial electron. In this case Eqs. (A1-3) yield,

Low Z limit: $Z\alpha << k$

$$\Delta\lambda \approx (1 - \cos\theta)(1 + |\varepsilon_0|). \quad \text{(A7)}$$

The change between Eqs. (A6) and (A7) is very notable; the Compton defect has become (for most purposes) much smaller, relative to the incident wavelength. This result agrees with the experimental findings in the present work. However, in order to check this finding more closely the functions f_1 and f_2 were evaluated in the specific cases studied here (see Table 1). In these cases no approximations of the kind used in Eqs. (A6) or (A7) really apply. However, all the results were still in keeping with Eq. (A7); that is the calculated Compton defects were so small ($\lesssim$5 keV) that they were undetectable. It is important to emphasize that all the above applies only to the centroid of the quasi-Compton peak. Where this peak is not observable or is significantly distorted due to energy considerations, interference from the IRD, or both, the simple classical approach utilized above cannot be applied.

References

1. M. Gavrila, *Phys. Rev.* 6A, 1348 (1972).
2. L. A. Wittwer, private communication. Available as UCRL-51268, August 1972.
3. I. B. Whittingham, *J. Phys. A*, 4, 21 (1971).
4. E. Storm and H. I. Israel, *Nuclear Data Tables* 7A, 1970.
5. J. Randles, *Proc. Phys. Soc.* A70, 337 (1957).
6. M. Schumacher, *Z. Physik* 242, 444 (1971).
7. D. Brini, E. Fuschini, N. T. Grimallni, and D. S. R. Murty, *Nuovo Cimento* 6, 727 (1960).
8. Z. Sujkowski and B. Nagel, *Arkiv Fur Fyski* 20, (19), 523 (1961).
9. J. Varma and M. A. Eswaran, *Phys. Rev.* 127, 1197 (1962).
10. S. Shimizu, Y. Nakayama, and T. Mukoyama, *Phys. Rev.* A140, 806 (1963).
11. L. V. East and E. R. Lewis, *Physica* 44, 595 (1969).
12. S. N. Chintalapudi and K. Parthusuradhi, *Indian J. Phys.* 43, 492 (1969).
13. D. S. R. Murty, D. V. Krishanreddy, and E. Narasimhacharyula, *Indian J. Phys. and Applied Phys.* 9, 305 (1970).
14. O. Pingot, *Le Journal De Physique* 33, 189 (1972).
15. J. W. Motz and G. Missoni, *Phys. Rev.* 124, 1458 (1961).
16. K. Siegbahn, *Alpha-, Beta-, and Gamma-Ray Spectroscopy*, (North Holland Publishing Company, Amsterdam, Netherlands, 1968), p. 293.
17. W. C. Heitler, *The Quantum Theory of Radiation*, (Oxford at the Clarendon Press, Oxford, 1954), p. 176.
18. J. M. Jauch and F. Rohrlich, *The Theory of Photons and Electrons*, (Addison-Wesley, Reading, Mass., 1955).
19. F. Bloch, *Phys. Rev.* 46, 674 (1934).
20. R. D. Evans, *Hand. d. Phys.* XXXIV, (Springer-Verlag, New York, 1958), p. 218.

GCS/lt/sg/lmc